On the Eccentricity Behaviour of Radiating Slowly Rotating Bodies in General Relativity

L. Herrera[*] [†]
Area de Física Teórica, *Facultad de Ciencias, Universidad de Salamanca,* 37008, Salamanca, España

H. Hernández[‡]
Laboratorio de Física Teórica,
Departamento de Física, Facultad de Ciencias, Universidad de Los Andes, Mérida 5101, Venezuela and
Centro Nacional de Cálculo Científico
Universidad de Los Andes
Corporación Parque Tecnológico de Mérida, Venezuela

L. A. Núñez[§]
Centro de Astrofísica Teórica,
Departamento de Física, Facultad de Ciencias, Universidad de Los Andes, Mérida 5101, Venezuela and
Centro Nacional de Cálculo Científico
Universidad de Los Andes
Corporación Parque Tecnológico de Mérida, Venezuela

and **U. Percoco**[¶]
Centro de Astrofísica Teórica,
Departamento de Física, Facultad de Ciencias, Universidad de Los Andes, Mérida 5101, Venezuela

August 1997

Abstract

We study different models of radiating slowly rotating bodies up to the first order in the angular velocity. It is shown that up to this order the evolution of the eccentricity is highly model-dependent even for very compact objects.

*On leave of absence from Centro de Astrofísica Teórica, Universidad de Los Andes, Mérida Venezuela , and Departamento de Física, Facultad de Ciencias U.C.V

†e-mail: lherrera@gugu.usal.es

‡e-mail: hector@ciens.ula.ve

§e-mail: nunez@ciens.ula.ve

¶e-mail: upercoco@ciens.ula.ve

1 Introduction

In recent papers by Gupta *et al* [1, 2], it has been shown that for a specific model of a slowly rotating object (up to the second order in angular velocity), the ellipticity attains a maximum for a surface gravitational potential, $\frac{M}{R} \approx 0.18$ (in geometric units).

This effect discovered by Chandrasekhar and Miller [3], and initially associated with frame dragging, was later related to the reversal of the centrifugal force in ultracompact objects. [4, 5].

In this work we study different models of radiating, (up to first order) slowly rotating objects. The motivation to undertake such a task is threefold:

- firstly, we want to check if the effect reported by Gupta and collaborators [1, 2], appears at first order. In this case the reversal of the centrifugal force (a second order effect), although may contribute to, has to be ruled out as the main cause of the maximum in the eccentricity.

- secondly, we would like to clarify if there exists a general tendency (model independent) in the evolution of eccentricity as the surface gravitational potential increases (see also [2] for a discussion on this point).

- finally, it is worth mentioning that the models presented in [1, 2] are only valid within the quasi-stationary approximation. In other words, their results are obtained by identifying the "history" of the evolution of the compact object with a sequence of stationary states. Instead we shall consider here systems which depart from hydrostatic equilibrium

As we shall see below, even for those cases of highly compact matter configurations, it appears that there is no model independent tendency for the eccentricity to attain a maximum. In one set of our simulations models start and end in a stationary state. It is obvious that in these cases the eccentricity reaches a constant value, but its value depends on the initial data considered. Several other simulations were preformed using two different equations of state. The models that emerge never reach stationary state. In these cases the eccentricity grows up continuously, even for surface gravitational potential as large as $\frac{M}{R} \approx 0.31$.

This paper is organized as follows. In the next section we introduce the conventions and give a brief description of the method employed to simulate the evolution of slowly rotating objects. Section 3 presents the three families of models considered. Finally, in the last section our results are discussed and contrasted with those obtained by Gupta and collaborators [1, 2].

2 The Formalism

Let us consider a nonstatic and axially symmetric distribution of matter formed by a fluid and radiation. The exterior metric, in radiation coordinates [6], takes the Kerr-Vaidya form [7]:

$$\begin{aligned} ds^2 &= \left(1-\frac{2mr}{r^2+\alpha^2\cos^2\theta}\right)\mathrm{d}u^2+2\mathrm{d}u\mathrm{d}r-2\alpha\sin^2\theta\mathrm{d}r\mathrm{d}\phi+ \\ &\quad +4\alpha\sin\theta^2\frac{mr}{r^2+\alpha^2\cos^2\theta}\mathrm{d}u\mathrm{d}\phi-(r^2+\alpha^2\cos^2\theta)\mathrm{d}\theta^2 \\ &\quad -\sin^2\theta\left[r^2+\alpha^2+\frac{2mr\alpha^2\sin^2\theta}{r^2+\alpha^2\cos^2\theta}\right]\mathrm{d}\phi^2\ . \end{aligned} \tag{1}$$

Here, α is the Kerr parameter, representing angular momentum per unit mass in the weak field limit, and m is the total mass. It is worth mentioning at this point that the metric above is not a pure radiation solution and may be interpreted as such only asymptotically [8]. A pure rotating radiation solution may be found in reference [9]. As we shall show below, although the interpretation of the Carmeli-Kaye metric is not completely clear, the model dependence of the considered effect is independent of the shape and the intensity of the emission pulse, and may be put in evidence even for a tiny radiated energy, $\Delta M_{rad} = 10^{-12}M(0)$, which for any practical purpose corresponds to the Kerr metric. The interior metric is written as [10]

$$\begin{aligned} ds^2 &= e^{2\beta}\left\{\frac{V}{r}\mathrm{d}u^2+2\mathrm{d}u\mathrm{d}r\right\}-(r^2+\tilde{\alpha}^2\cos^2\theta)\mathrm{d}\theta^2 \\ &\quad +2\tilde{\alpha}e^{2\beta}\sin^2\theta\left\{1-\frac{V}{r}\right\}\mathrm{d}u\mathrm{d}\phi-2e^{2\beta}\tilde{\alpha}\sin^2\theta\mathrm{d}r\mathrm{d}\phi \\ &\quad -\sin^2\theta\left\{r^2+\tilde{\alpha}^2+2\tilde{\alpha}^2\sin^2\theta\frac{V}{r}\right\}\mathrm{d}\phi^2\ . \end{aligned} \tag{2}$$

In equations (1) and (2), $u = x^0$ is a time like coordinate, $r = x^1$ is the null coordinate and $\theta = x^2$ and $\phi = x^3$ are the usual angle coordinates. The u-coordinate is the retarded time in flat space-time and, therefore, u-constant surfaces are null cones open to the future.

The Kerr parameter for the interior space-time (2) is denoted $\tilde{\alpha}$ and, for the present work and for sake of simplicity, will be considered constant and relevant only (as well as α in eq. (1)) up to the *first order*. Notice that in these coordinates the $r = constant = r_s$ surfaces are not spheres but *oblate spheroids*, whose eccentricity depends upon the Kerr parameter $\tilde{\alpha}$ and is given by

$$e^2 = 1-\frac{r_s^2}{r_s^2+\tilde{\alpha}^2}\ , \tag{3}$$

with r_s representing the shell where the eccentricity is evaluated. Observe that eccentricity as defined by (3), although it yields the correct Newtonian limit and is the natural definition in the context of metrics (1) and (2), is not invariantly defined . However the main argument to use it here, stems from the fact that it is that parameter the one whose evolution is studied in references [1, 2].

The metric elements β and V in eq. (2), are functions of u, r and θ. A function $\tilde{m}(u, r, \theta)$ can be defined by

$$V = e^{2\beta}\left(r - \frac{2\tilde{m}(u, r, \theta)r^2}{r^2 + \tilde{\alpha}^2\cos^2\theta}\right) , \tag{4}$$

which is the generalization, inside the distribution, of the "mass aspect" defined by Bondi and collaborators [11] and in the static limit coincides with the Schwarzschild mass.

In this work the modeling is performed by means of a general method presented a few years ago [12], which allows the generation of axially symmetric slowly rotating (up to the first order), radiating solutions from known static "seed" solutions.

Only a very brief description of the method is given here, we refer the reader to [12] for details.

The method starts by defining two auxiliary functions

$$\tilde{\rho} = \frac{\rho - P\omega_x}{1 + \omega_x} \tag{5}$$

and

$$\tilde{P} = \frac{P - \rho\omega_x}{1 + \omega_x} . \tag{6}$$

which are called the *effective variables*. In equations (5) and (6) ω_x represents the radial component of the velocity of a fluid element as measured by a local minkowskian observer. Also in the above equations the physical (local) pressure and density are denoted by ρ and P.

Next, it can be easily shown using the field equations that the metric elements $\tilde{m}$ and β can be expressed as

$$\tilde{m} = \int_0^r \mathrm{d}\bar{r} 4\pi\bar{r}^2\tilde{\rho} \tag{7}$$

and

$$\beta = \int_r^{a(u)} \frac{2\pi\bar{r}^2\mathrm{d}\bar{r}}{\bar{r} - 2\tilde{m}}\left(\tilde{\rho} + \tilde{P}\right) . \tag{8}$$

where $r = a(u)$ is the equation of the boundary surface.

It is clear that, if the radial dependence of $\tilde{\rho}$ and $\tilde{P}$ are borrowed from the "seed" static solution, the metric elements $\tilde{m}$ and β , can be determined from eq. (7) and (8), up to some functions of the time-like coordinate u. In the context

of this approach the radial dependence of $\tilde{\rho}$ and $\tilde{P}$ is assumed to be the same as in the static "seed" solution.

The rationale behind the assumption on the r dependence of the *effective variables* $\tilde{P}$ and $\tilde{\rho}$, can be grasped in terms of the characteristic times for different processes involved in a collapse scenario. If the hydrostatic time scale $\mathcal{T}_{HYDR}$, which is of the order $\sim 1/\sqrt{G\rho}$ (where G is the gravitational constant and ρ denotes the mean density) is much smaller than the *Kelvin-Helmholtz* time scale ($\mathcal{T}_{KH}$), then in a first approximation the inertial terms in the equation of motion can be ignored [13] . Therefore in this first approximation (quasi-stationary approximation) the r dependence of P and ρ are the same as in the static solution. Then the assumption that the *effective variables* (5) and (6) have the same r dependence as the physical variables of the static situation, represents a correction to that approximation, and is expected to yield good results whenever $\mathcal{T}_{KH} \gg \mathcal{T}_{HYDR}$. Fortunately enough, $\mathcal{T}_{KH} \gg \mathcal{T}_{HYDR}$, for almost all kind of stellar objects.

Those functions of the time-like coordinate u that remain arbitrary can be obtained from a system of ordinary differential equations (*The System of Surface Equations*) emerging from the field equations evaluated at the boundary surface and the junction conditions.

The equations corresponding to the junction conditions (eq. (49), and (50) in [12]) lead to

$$\beta_{1a}\,(1+\dot{a}) = f(u)\alpha \tag{9}$$

and

$$\tilde{m}_{1a}\,(1+\dot{a}) = g(u)\alpha\ . \tag{10}$$

Where $f(u)$ and $g(u)$ are arbitrary functions of their arguments, differentiation with respect to u and r are denoted by subscripts 0 and 1, respectively and the subscript a indicates that the quantity is evaluated at the boundary surface. Finally, in radiation coordinates, $\dot{a}$ takes the form

$$\dot{a} = \frac{\mathrm{d}a}{\mathrm{d}u} = \frac{\omega_{xa}}{1-\omega_{xa}}\left(1-\frac{2\tilde{m}_a}{a}\right)\ . \tag{11}$$

Also, from the junctions conditions (eq. (40) in [12]) we get,

$$\beta_{1a}\left(1-\frac{2\tilde{m}_a}{a}\right) - \beta_{0a} = \frac{\tilde{m}_{1a}}{2a} \quad , \tag{12}$$

or equivalently

$$2a\beta_{1a}\left(1+\dot{a}-\frac{2\tilde{m}_a}{a}\right) = \tilde{m}_{1a} \tag{13}$$

From equations (13), (9) and (10) we obtain an expression relating $f(u)$ and $g(u)$, namely

$$2a\left(1+\dot{a}-\frac{2\tilde{m}_a}{a}\right) f(u) = g(u)\ . \tag{14}$$

However, it can be checked by simple inspection that neither the field equations nor the junction conditions impose further restrictions on these functions of u, therefore one of them remains completely arbitrary for each model.

Expanding (3) for $\tilde{\alpha} \ll 1$, we get

$$e = \frac{1}{r_s}\tilde{\alpha} - \frac{1}{2}\frac{1}{r_s^3}\tilde{\alpha}^3 + \cdots \ , \tag{15}$$

thus, as expected, up to first order the eccentricity is proportional to $\tilde{\alpha}$. Now equations (10) and (14) lead to

$$\tilde{\alpha} = \frac{\tilde{m}_{1a}\,(1+\dot{a})}{2a\left(1+\dot{a}-\frac{2\tilde{m}_a}{a}\right)f(u)} \tag{16}$$

or, using eq. (7),

$$\tilde{\alpha} = 2\frac{\pi a\tilde{\rho}_a(u)\,(1+\dot{a})}{\left(1+\dot{a}-\frac{2\tilde{m}_a}{a}\right)f(u)} \ . \tag{17}$$

It is easy to see that two different types of variables are needed to determine $\tilde{\alpha}$ from (17). On one hand, we notice $a, \dot{a}, \tilde{\rho}_a$, and $\tilde{m}_a$ which can be obtained from the integration of the *Surface Equations* and the particular "seed" solution selected to be modeled. On the other hand, as we have stated before, $f(u)$ remains completely arbitrary and its choice completes the characterization of the model.

In the next section we shall present three different families of models obtained from different static equations of state.

3 The Modeling

In order to show that there is no model independent tendency for the eccentricity to attain a maximum, we shall consider three different families of equations of state. Each one will be modeled with three different choices of the arbitrary function $f(u)$. We shall work out three models, previously studied for the spherical (nonrotating) case: *Schwarzschild-like*[14, 15], *Tolman-VI-like* [14, 15] and *Tolman-V-like* [14, 16, 17] solutions. In the static limit the *Schwarzschild-like* homogeneous solution represents an incompressible fluid of constant density. Static *Tolman VI* solution approaches that of a highly relativistic Fermi Gas and, therefore, with the corresponding adiabatic exponent of 4/3. And, for the static *Tolman V* solution, the radiation relation $P/\rho \sim 1/3$, is maintained at the center of the distribution during the contraction.

All the above equations of state will be used as a "seed" solution to study the evolution of the eccentricity. The first family to be considered is the Schwarzschild solution. It is the same example presented in ref. [12].

$$\tilde{\rho} = k(u) = \frac{3}{8\pi}\frac{(1-F(u))}{A(u)^{\ 2}} \ , \tag{18}$$

and

$$\tilde{\alpha} = \frac{3\,(1-\,F(u))\,(1+F(u)\,(\Omega(u)-1))}{4\,A(u)\;F(u)\;\Omega(u)\;f(u)}\;; \tag{19}$$

where the exterior radius a, the total mass m, and the timelike coordinate u are scaled by the initial total mass $m(u\,=\,0)\,=\,m(0)$, i.e. $A\,=\,a/m(0)$; $M = m/m(0)$ and $u = u/m(0)$. We have also defined

$$F(u) = 1 - \frac{2M(u)}{A(u)} \tag{20}$$

and

$$\Omega(u) = \frac{1}{1-\omega_{xa}}\;. \tag{21}$$

The second case is the slowly rotating *Tolman-V-like* models. In this case we have

$$\tilde{\rho} = \frac{1}{8\pi}\left(\frac{\delta(u)}{r^2} + z(u) r^{\frac{1}{3}}\right) \tag{22}$$

where

$$\tilde{\alpha} = \frac{(1-F(u))\,(1+F(u)\,(\Omega(u)-1))}{3\;\;A(u)\;F(u)\;f(u)}\;. \tag{23}$$

with

$$\delta(u) = \frac{2}{7}\,(F(u)-1)\,(2\,\Omega(u)-5) \tag{24}$$

and

$$z(u) = \frac{10}{21\,A(u)^{7/3}}\,(1-F(u)\,)\,(4\,\Omega(u)-3)\,. \tag{25}$$

Finally we take the *Tolman VI-like* family of models, with the effective density represented by

$$\tilde{\rho} = \frac{3h(u)}{r^2} = \frac{1}{8\pi}\frac{(1-F(u))}{r^2} \tag{26}$$

and for the eccentricity we have found

$$\tilde{\alpha} = \frac{(1-F(u))\,(1+F(u)\,(\Omega(u)-1))}{4\,A(u)\;F(u)\;\Omega(u)\;f(u)}. \tag{27}$$

As we have mentioned above, the evolution of these three families of eccentricities (19), (27), (23) have been calculated for three different expressions of $f(u)$, namely:

$$f(u) = \begin{cases} cte = 1 \\ 1+u \\ 1 + C\exp - \left(\frac{u-u_{trig}}{\sigma}\right)^2 \end{cases} \tag{28}$$

with u_{trig} a triggering parameter, C a modulation constant and σ the width of the pulse.

Simulations have been carried out for a large number of sets of initial data and emission pulses. We shall present in the next section only the most relevant cases.

The radiation flux has been assumed to be in the *free streaming out limit* approximation, i.e. neutrinos and/or photons mean free path is of the order of the dimensions of the spheroid. It is worth mentioning that for the modeling performed, the shape and the intensity of the emission pulse does not seem to play an important role, we shall only exhibit the results obtained with a Gaussian pulse centered at $u = u_p$

$$-\dot{M} = L = \frac{\Delta M_{rad}}{\lambda\sqrt{2\pi}} \exp \frac{1}{2}\left(\frac{u-u_p}{\lambda}\right)^2, \tag{29}$$

with λ the width of the pulse and ΔM_{rad} the total mass lost in the process. All models presented in the next section have been simulated using

$$\Delta M_{rad} = 0.001 \qquad \lambda = 0.1 \qquad u_p = 15 \tag{30}$$

The sets of initial data relevant to be discussed are:

- *Schwarzschild-like* (displayed in Figures 1 and 2)

$$\frac{M(0)}{A(0)} = 0.185; \quad \Omega(0) = 0.933; \quad A(0) = 5.404; \quad F(0) = 0.630 \tag{31}$$

  and

$$\frac{M(0)}{A(0)} = 0.303; \quad \Omega(0) = 0.933; \quad A(0) = 3.300; \quad F(0) = 0.394 \tag{32}$$

- *Tolman V-like* (displayed in Figure 3)

$$\frac{M(0)}{A(0)} = 0.217; \quad \Omega(0) = 0.809; \quad A(0) = 4.600; \quad F(0) = 0.565 \tag{33}$$

- *Tolman VI-like* (displayed in Figure 4)

$$\frac{M(0)}{A(0)} = 0.270; \quad \Omega(0) = 1.000; \quad A(0) = 3.700; \quad F(0) = 0.459 \tag{34}$$

The running time for the models (values for u) are controlled by the physical relevance of the variables involved. As we shall see in the next section the behavior of $\tilde{\alpha}$ is highly model dependent, no matter how compact the object becomes.

4 Discussion of Results

Let us start by analyzing the *Schwarzschild-like* model. Figures 1a through 1c display the evolution of the eccentricity for the above mentioned choices of $f(u)$ in equation (28) with the set of initial data (31). Figure 1d indicates the evolution of $F(u)$. Observe that cases

$$f(u) = \begin{cases} cte = 1 \\ 1 + C \exp - \left(\frac{u - u_{trig}}{\sigma} \right)^2 \end{cases} \tag{35}$$

yield results very similar to those reported in [1] although we are considering only first order terms ! These result are presented in Figures 1a and 1c, respectively. From Figures 1a, 1c and 1d we can see that the eccentricity for the above two cases present a maximum when the surface gravitational potential reaches

$$\frac{M(u)}{A(u)} = \frac{1}{2} \left(1 - F(u) \right) \approx 0.18 \; . \tag{36}$$

The other model, corresponding to the case $f(u) = 1 + u$ also gives a stationary value for the eccentricity for the above value for the gravitational potential at the surface of the configuration.

Thus, up to the first order this model would seem to confirm the result found in [1, 2]. However, this is not so. Indeed, Figures 2a to 2d represent the evolution of the eccentricity, $e(u)$, and $F(u)$, for another set of initial data (see equations (32)). Now the stationary value for $e(u)$ is obtained for $\frac{M(u)}{A(u)} \approx 0.33$. It is worth noticing that for a given set of initial data the final value of $e(u)$ is independent of the $f(u)$.

Let us now turn to consider the *Tolman V-like* family of models with the set of initial data (33). Figures 3a through 3c exhibit the evolution of the eccentricity concerning the functions $f(u)$ in equation (28). In Figure 3d the evolution of $F(u)$ is displayed. As it is apparent from these figures, there is no maximum in the value of the eccentricity, even though the surface gravitational potential goes well beyond the supposed critical value of $\frac{M(u)}{A(u)} \approx 0.18$ (see Figure 3d).

Finally, Figures 4a to 4d refer to *Tolman VI-like* family of models, and point in the same direction as the previous case. In fact, Figures 4a to 4c show that either the eccentricity grows up continuously ($f(u)$ is one of the above eq. (35)) or attains a minimum and grows up again ($f(u) = 1 + u$), even though the surface gravitational potential may reach values as high as $\frac{M(u)}{A(u)} \approx 0.31$ (Figure 4d).

Summarizing our results. It is clear that, up to the first order in angular parameters, the evolution of the eccentricity is highly model dependent. If second order contributions are going to be considered, they should be assumed much smaller than the first order ones. Therefore, it is not reasonable to expect

that second order contributions could bend the curves displayed in Figures 3a, 3c, 4a and 4c as to create a maximum for $e(u)$ or that they can subdue the dependence of the final value of $e(u)$ on the initial data for the *Schwarzschild-like* models. In other words, we can not see how the second order effects might affect qualitatively the model dependence exhibited here.

Of course, it remains to be seen whether the effects described in [1, 2] appear in a model independent way in the exact theory of relativistic rotating bodies. For that purpose, however, we would need an exact interior solutions for the axially symmetric source, which, as it is well known, is not available yet.

We would like to conclude with the following comment. Although the main purpose here has been to bring out the model dependence of the evolution of the eccentricity, and not specific modeling of rotating sources, it should be noticed that in the examples above the energy density is always positive and larger than pressure everywhere within the fluid distribution and the fluid velocity as measured by the locally Minkowskian observer is always less than one. Although we do not include figures of physical variables (some of them for the case $f = 1$ may be found in reference [12]), the reader may convince himself of that by noticing that the three models considered here have been studied in detail in the spherically symmetric case [15, 16, 17], in which all models have a correct physical behaviour. Of course we do not expect that first order perturbation may change that situation.

Two of us (H.H. and L.A.N) gratefully acknowledge the financial support by the Consejo de Desarrollo Científico Humanístico y Tecnológico de la Universidad de Los Andes, under project C-720-95-B and by the Programa de Formación e Intercambio Científico (Plan II).

References

[1] Gupta, A., Iyer, S., and Prasannsa, A. 1996, *Class. Quantum Grav.,* **13**, 2675.

[2] Gupta, A., Iyer, S., and Prasannsa, A. 1997, *Class. Quantum Grav.,* **14**, L143.

[3] Chandrasekhar, S. and Miller, J.C. 1974, *Mon. Not. R. Astron. Soc.,* **167**, 63.

[4] Abramowicz, M. A. and Prasanna, A. R. 1990, *Mon. Not. R. Astron. Soc.,* **245**, 720.

[5] Abramowicz, M. A. and Miller, J.C., 1990, *Mon. Not. R. Astron. Soc.,* **245**, 729.

[6] Bondi, H., 1964 *Proc. Roy. Soc. London,* **281,** 39.

[7] Carmeli, M. and Kaye, M. 1977 *Ann. Phys. (N.Y.),* **103,** 97.

[8] González, C., Herrera, L. and Jiménez J. 1979, *J.Math.Phys.*, **20**, 836.

[9] Kramer, D. and Hahner, U. 1995, *Class.Quantum.Grav.*, **12**, 2287.

[10] Herrera, L. and Jiménez, J. 1982, *J. Math Phys.*, **23,** 2339.

[11] Bondi, H., Van der Burg, M. G. J. and Metzner, A. W. K., 1962. *Proc R. Soc. London,* **A269**, 21.

[12] Herrera, L., Melfo, A., Núñez, L.A. and Patiño, A. 1994 *Astrophys. J.* 421, 677.

[13] Kippenhahn, R. and Weigert, A. 1990, *Stellar Structure and Evolution*, (Springer Verlag, Berlin), p. 11.

[14] R. C. Tolman.: 1939, *Phys. Rev.* **55**, 364.

[15] Herrera, L., Jiménez, J. and Ruggeri, G. 1980. *Phys. Rev.* **D22** 2305.

[16] Patiño, A. and Rago, H.: 1983, *Lett. Nuovo Cimento* **38**, 321.

[17] Aguirre, F., Hernández, H. and Núñez L.A. 1994, *Astrophys and Space Sc.* **219,** 153.

Figure Captions

Figure 1 The evolution of the eccentricity for the *Schwarzschild-like* model with $\frac{M(0)}{A(0)} = 0.185$. Figures 1a through 1c correspond to functions: $f(u) = cte = 1$; $f(u) = 1 + u$; and $f(u) = 1 + C \exp - \left(\frac{u - u_{trig}}{\sigma}\right)^2$, respectively. Figure 1d indicates the evolution of the gravitational potential at the surface: $F(u) = 1 - \frac{2M(u)}{A(u)}$.

Figure 2 The evolution of the eccentricity for the *Schwarzschild-like* model with $\frac{M(0)}{A(0)} = 0.303$. Figures 2a through 2c correspond to functions: $f(u) = cte = 1$; $f(u) = 1 + u$; and $f(u) = 1 + C \exp - \left(\frac{u - u_{trig}}{\sigma}\right)^2$, respectively. Figure 2d indicates the evolution of the gravitational potential at the surface: $F(u) = 1 - \frac{2M(u)}{A(u)}$.

Figure 3 The evolution of the eccentricity for the *Tolman V-like* model with $\frac{M(0)}{A(0)} = 0.217$. Figures 3a through 3c correspond to functions: $f(u) = cte = 1$; $f(u) = 1 + u$; and $f(u) = 1 + C \exp - \left(\frac{u - u_{trig}}{\sigma}\right)^2$, respectively. Figure 3d indicates the evolution of the gravitational potential at the surface: $F(u) = 1 - \frac{2M(u)}{A(u)}$

Figure 4 The evolution of the eccentricity for the *Tolman VI-like* model with $\frac{M(0)}{A(0)} = 0.270$. Figures 4a through 4c correspond to functions: $f(u) = cte = 1$; $f(u) = 1 + u$; and $f(u) = 1 + C \exp - \left(\frac{u - u_{trig}}{\sigma}\right)^2$, respectively. Figure 4d indicates the evolution of the gravitational potential at the surface: $F(u) = 1 - \frac{2M(u)}{A(u)}$

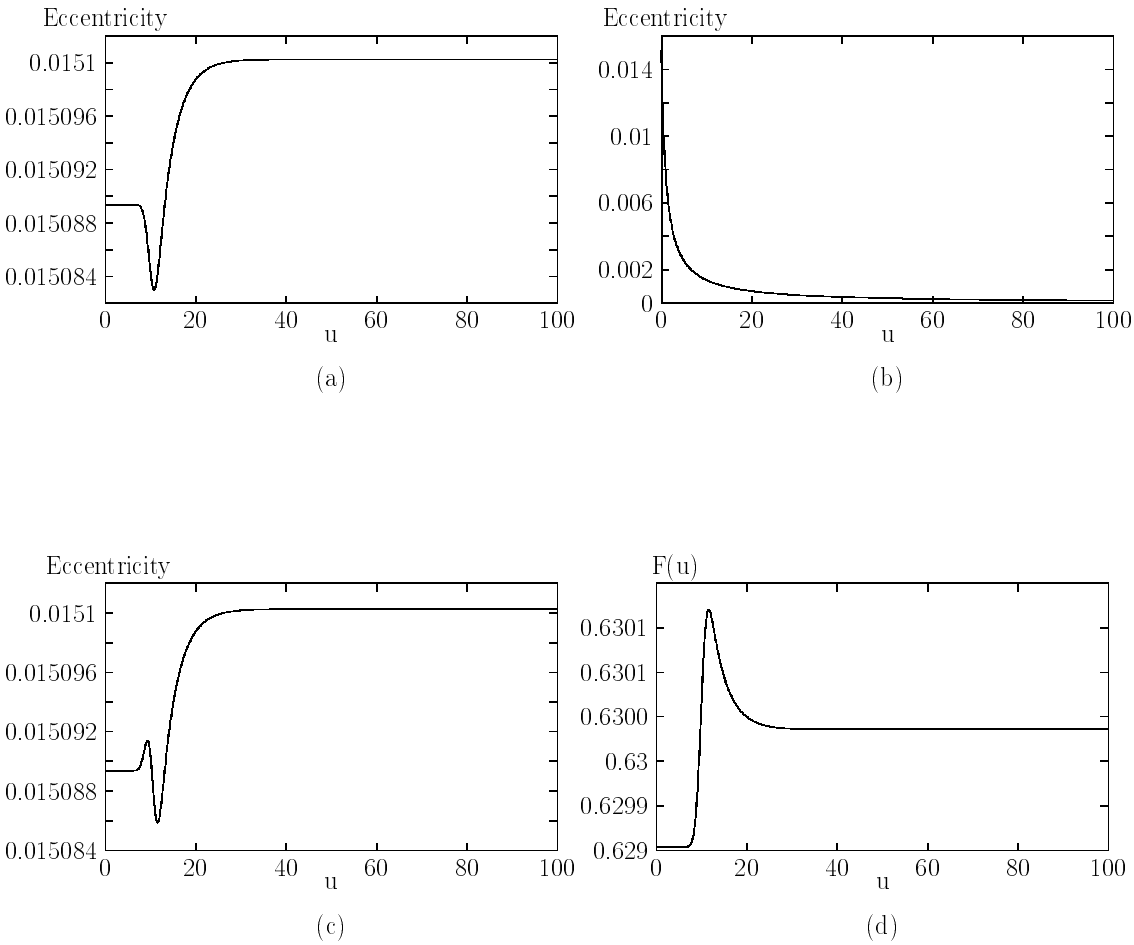

Figure 1:

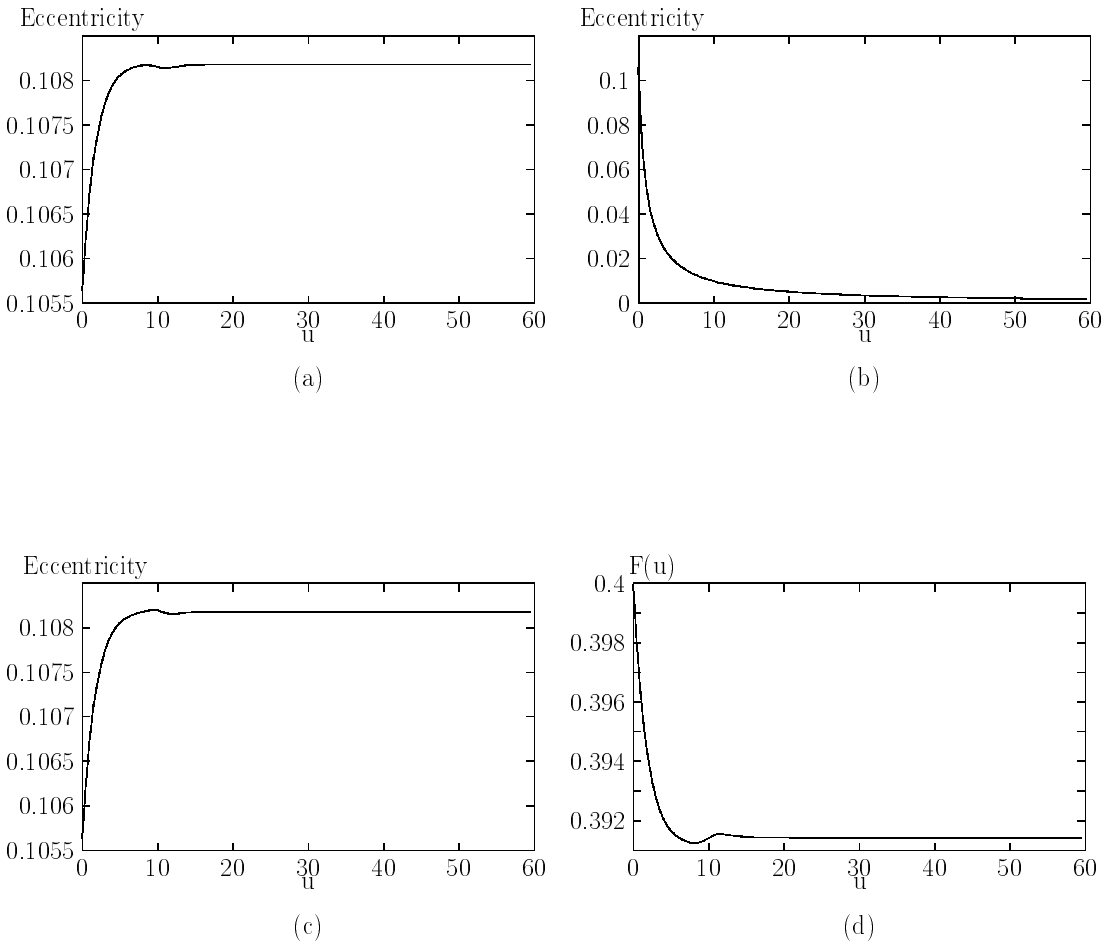
Eccentricity
0.108
0.1075
0.107
0.1065
0.106
0.1055
0
10
20
30
40
50
60
u
(a)
Eccentricity
0.1
0.08
0.06
0.04
0.02
0
u
(b)
Eccentricity
0.108
0.1075
0.107
0.1065
0.106
0.1055
u
(c)
F(u)
0.4
0.398
0.396
0.394
0.392
u
(d)

Figure 2:

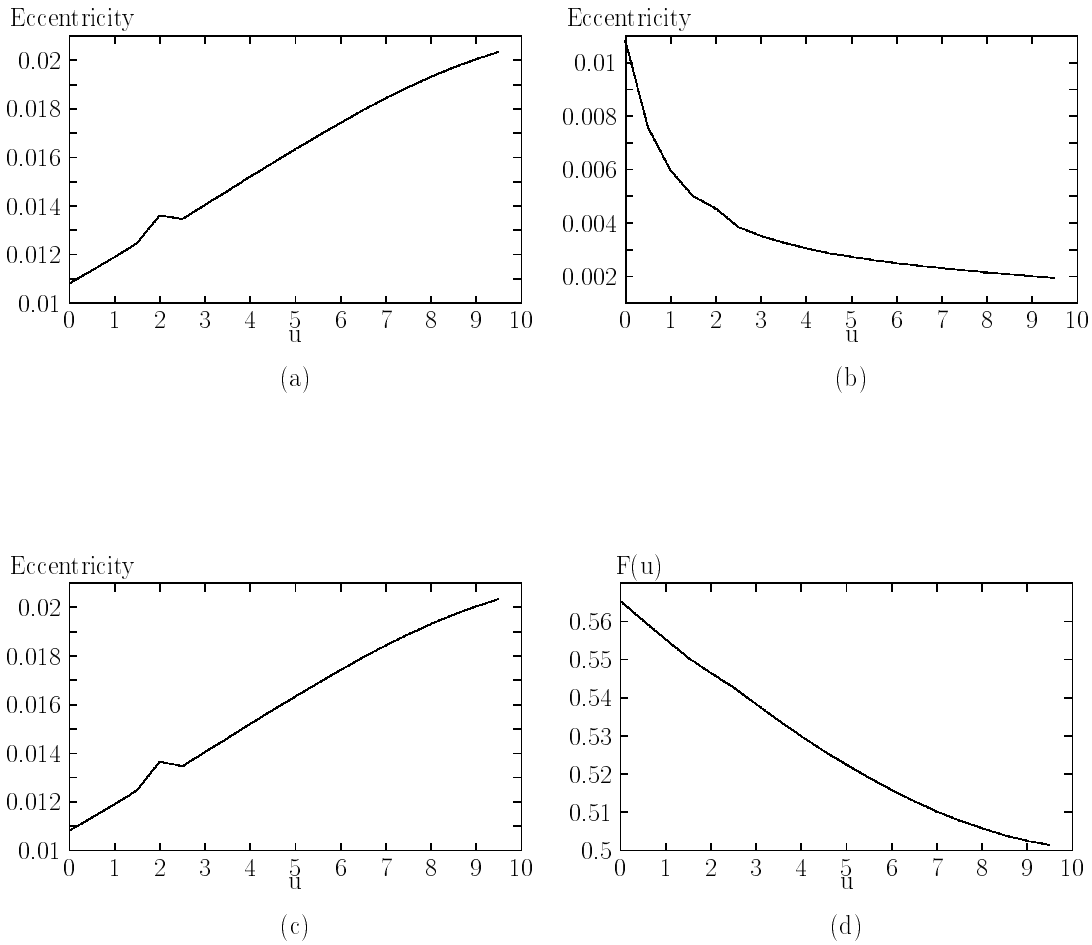
Eccentricity
0.02
0.018
0.016
0.014
0.012
0.01
0 1 2 3 4 5 6 7 8 9 10
u
(a)
Eccentricity
0.01
0.008
0.006
0.004
0.002
0 1 2 3 4 5 6 7 8 9 10
u
(b)
Eccentricity
0.02
0.018
0.016
0.014
0.012
0.01
0 1 2 3 4 5 6 7 8 9 10
u
(c)
F(u)
0.56
0.55
0.54
0.53
0.52
0.51
0.5
0 1 2 3 4 5 6 7 8 9 10
u
(d)

Figure 3:

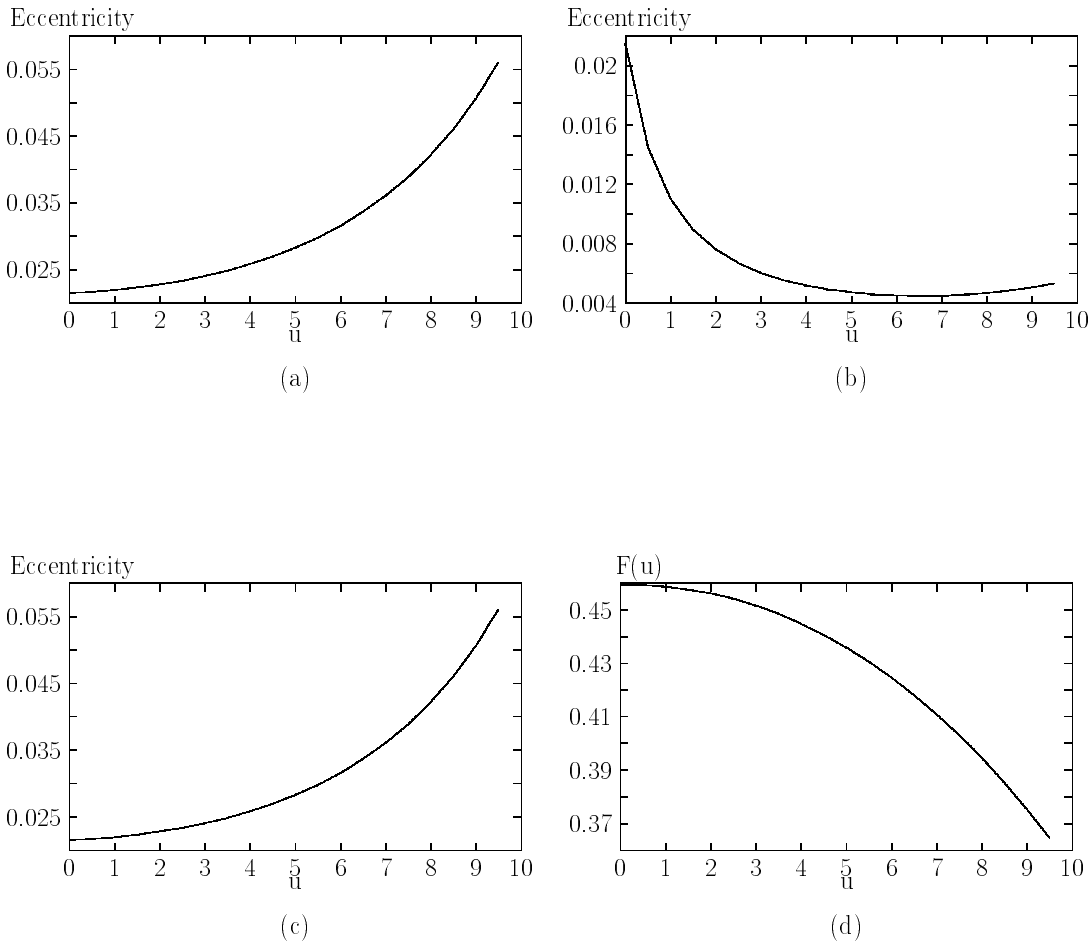
Eccentricity
0.055
0.045
0.035
0.025
0 1 2 3 4 5 6 7 8 9 10
u
(a)
Eccentricity
0.02
0.016
0.012
0.008
0.004
0 1 2 3 4 5 6 7 8 9 10
u
(b)
Eccentricity
0.055
0.045
0.035
0.025
0 1 2 3 4 5 6 7 8 9 10
u
(c)
F(u)
0.45
0.43
0.41
0.39
0.37
0 1 2 3 4 5 6 7 8 9 10
u
(d)

Figure 4: